



## Characterisation of electrochemically grown $\text{In}_x\text{Se}_y$ thin films for application in photonic devices

M.L. Madugu<sup>1,2\*</sup>, O.I. Olusola<sup>1,3</sup>, A.A. Ojo<sup>1</sup>, N.Y. Pindiga<sup>4</sup>

<sup>1</sup>Electronic Materials and Sensors group, Materials and Engineering Research Institute, Sheffield Hallam University, Sheffield, S1 1WB, UK.

<sup>2</sup>Department of Physics, Faculty of Science, Gombe State University, Tudun Wada, P.M.B. 127, Gombe, Nigeria

<sup>3</sup>Department of Physics, School of Science, The Federal University of Technology, Akure, Ondo State, P.M.B. 704, Nigeria.

<sup>4</sup>Department of Chemistry, Faculty of Science, Gombe State University, Tudun Wada, P.M.B 127, Gombe, Nigeria

Received 04 Nov 2017,  
Revised 13 May 2018,  
Accepted 20 May 2018

### Keywords

- ✓  $\text{In}_x\text{Se}_y$
- ✓ Electrodeposition
- ✓ n-type and p-type
- ✓ Amorphous

[maduguu@yahoo.com](mailto:maduguu@yahoo.com)  
+2349068697538

### Abstract

Indium selenide ( $\text{In}_x\text{Se}_y$ ) layers were grown on glass/FTO substrates using electrodeposition technique in a potentiostatic mode. After growth, the materials were characterised for their structural, optical and electrical properties. Structural studies show that the material is amorphous with no  $\text{In}_x\text{Se}_y$  peak as revealed by the X-ray diffraction (XRD) spectra. Optical studies using ultraviolet visible (UV-Vis) spectrophotometer show that the material bandgap increased from 2.45 eV in the as-deposited and increased to 2.90 eV after annealing. Electrical studies on the conductivity type of the  $\text{In}_x\text{Se}_y$  thin films show that, both n-type and p-type  $\text{In}_x\text{Se}_y$  layers were grown by simply varying the growth potential. Materials deposited at low growth voltages are p-type in electrical conduction while those grown at higher potentials show n-type electrical conduction.

## 1. Introduction

Indium selenide ( $\text{In}_x\text{Se}_y$ ) is a layered III-VI semiconductor material with a direct energy bandgap of 1.80 eV at room temperature [1]. However, the bandgap is tuneable depending on the growth and post growth processes. The basic structure of  $\text{In}_x\text{Se}_y$  layers were made from two *In* and two *Se* sublayers and the interlayer (Se-Se) bonding is of the Van der Waals type. Due to this bonding structure, there exist less dangling bonds at the surface which provides ideal condition for fabricating metal-semiconductor or p-n hetero-junctions. Thus, the interfaces between such layered materials are unstrained even for the relatively high lattice mismatches [2].  $\text{In}_x\text{Se}_y$  is a complicated system due to its multiphase nature. It can exist in different phases such as  $\text{InSe}$ ,  $\text{In}_2\text{Se}_3$ ,  $\text{In}_4\text{Se}_3$  and  $\text{In}_6\text{Se}_7$  [3].  $\text{In}_x\text{Se}_y$  can exist as both n-type [4,5] and p-type [1,6] in electrical conduction depending on the growth conditions. This material is attractive due to its optoelectronic properties and have found applications in areas such as solar cells [2,7], switching devices [8], radiation detectors [9] and gas sensors [10].  $\text{In}_x\text{Se}_y$  is deposited using variety of techniques such as Bridgeman-Stockbarger [5], electrodeposition [11], and thermal evaporation [12] among others.

The low density of dangling bonds on the surface of layered semiconductors such as  $\text{In}_x\text{Se}_y$  and GaSe makes them very good materials for the fabrication of hetero-junction devices [13] with minimum lattice mismatch [14–16]. Cadmium sulphide (CdS) is up till now the best hetero-junction partner in both CIGS and CdTe-based solar cells. The incorporation of CdS as a buffer/window layer in both device structures yielded efficiencies in excess of 21% [17]. However, due to health and environmental issues, it is important to replace CdS with less toxic alternative buffer materials such as ZnSe,  $\text{ZnIn}_x\text{Se}_y$  and  $\text{In}_x\text{Se}_y$ . Gordillo and Calderon incorporated  $\text{In}_x\text{Se}_y$  in ZnO/ $\text{InSe}$ /CIS/Mo solar cell structure achieving 9.2% efficiency, Konagai *et al.* [18] incorporated  $\text{In}_x\text{Se}_y$  as a buffer layer in ZnO/ $\text{In}_x\text{Se}_y$ /CIGS solar cell with cell efficiency of 13%. This indicates why  $\text{In}_x\text{Se}_y$  will be a good candidate for incorporation as buffer layer in multi-layer graded bandgap devices based on CdTe and CIGS solar cells. The work presented in this communication examined some material properties of  $\text{In}_x\text{Se}_y$  layers for application in photonic devices.

## 2. Material and Methods

### 2.1. Materials

All chemicals and other materials were purchased from Sigma-Aldrich, UK.

### 2.2. Preparation of $In_xSe_y$ thin films

The electrolyte for the deposition of  $In_xSe_y$  was prepared from 0.1 M  $InCl_3$  of purity 5N (99.999%) and 0.025 M  $SeO_2$  of purity 5N (99.999%) which are the sources of indium (In) and selenium (Se) respectively. The chemicals were dissolved in 200 ml aqueous solution of deionised water. The pH of the electrolyte was adjusted to  $1.50 \pm 0.02$  at room temperature using HCl or  $NH_4OH$ . The temperature of the bath was set at  $\sim 40^\circ C$  before deposition.

To remove grease and other contaminants on the glass/FTO substrates, they were first washed with soap solution and rinsed in deionised water. Then the substrates were cleaned with methanol followed by deionised water. The working electrode (glass/FTO) was attached to a carbon rod using polytetrafluoroethylene (PTFE) tape while the anode is a high purity carbon rod; the two electrodes were suspended vertically inside the electrolyte during deposition. The deposition was done in aqueous acidic solution using 2-electrode system in a cathodic mode (as shown in Figure 1). The heat was provided by hot plate with attached stirring system and the source of power was a Gill AC potentiostat (ACM instrument).

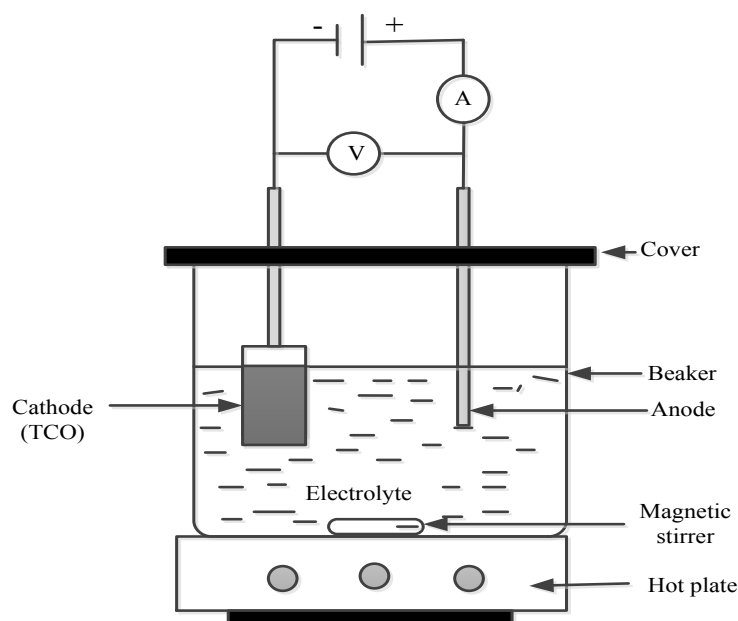


**Figure 1:** Two- electrode (2E) electroplating system set-up.

### 2.3. Methods

The structural properties of the films were studied using Philips X' Pert Pro diffractometer (Philips analytical) with  $Cu-K_\alpha$  radiation source with excitation of  $1.541 \text{ \AA}$ . Optical absorption measurements were studied using Cary 50 UV-Vis spectrophotometer. Scanning electron microscopy images were taken using FEI Nova 200 NanoSEM. The conductivity types of the films were studied using photoelectrochemical (PEC) cell measurement system.

## 3. Results and discussion

### 3.1 Cyclic voltammetry

In electrodeposition, the cyclic voltammetry is a tool used to investigate the approximate deposition potential window for a near stoichiometric material. Figure 2 depicts the current-voltage (I-V) relationship (voltammogram) obtained for the reduction of  $In_xSe_y$  compound on glass/FTO cathode. The temperature of the bath was set to  $\sim 40^\circ C$ , and the voltammogram was recorded for voltage range (0 to 2000) mV and back to 0 with scan rate of  $3 \text{ mVs}^{-1}$ .

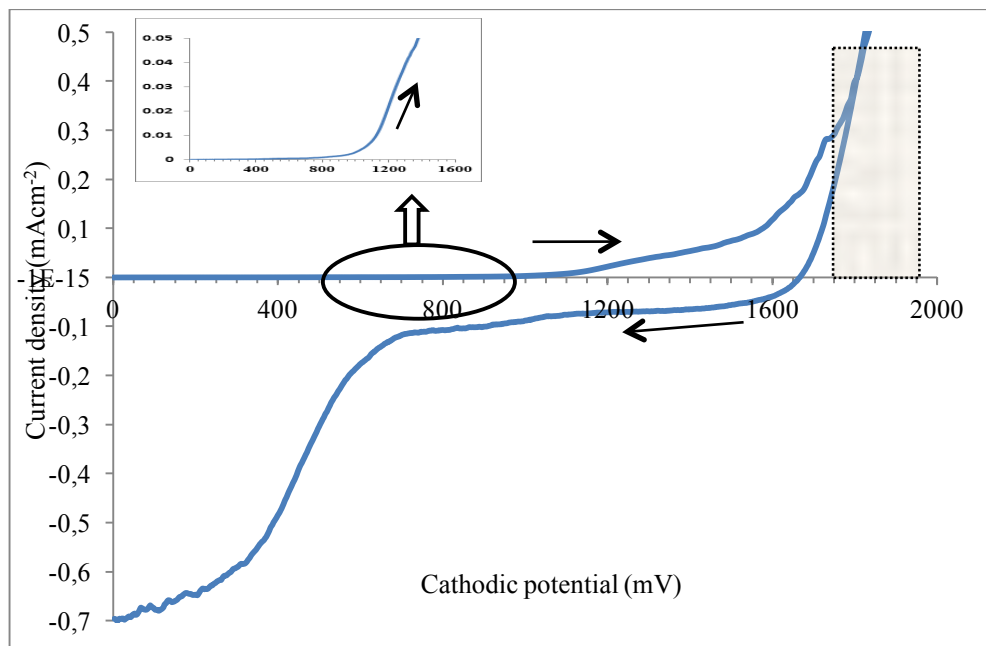


**Figure 2:** Cyclic voltammogram of aqueous solution containing 0.1 M  $\text{InCl}_3$  + 0.025 M  $\text{SeO}_2$ , with glass/FTO cathode and graphite anode. The pH and temperature of the electrolyte were  $1.50 \pm 0.02$  and  $\sim 40^\circ\text{C}$  respectively.

Looking at Figure 2 and with reference to the reduction potentials ( $E^0$ ) of the constituent ions, ( $E^0$  of  $\text{Se} = +0.740$  V, and  $E^0$  of  $\text{In} = -0.338$  V) [19], This means that  $\text{Se}$  with the low reduction potential is first deposited at low cathodic voltages while  $\text{In}$  with the higher reduction potential will reduce at higher cathodic voltages.  $\text{Se}$  will start to reduce on the cathode at voltage around 550 mV as is clearly seen from the inset diagram of Figure 2. A steady increase in deposition current from cathodic voltage around 1000 mV could be due to the incorporation of  $\text{In}$  on the cathode. The approximate deposition potential for near stoichiometric  $\text{In}_x\text{Se}_y$  is expected within the voltage range (1750-1950) mV as indicated by the shaded portion of the voltammogram. At larger cathodic voltages greater than 1950 mV,  $\text{In}$  is reduced instead of the desired  $\text{In}_x\text{Se}_y$ . This voltage region produced poor film quality which cannot withstand device processing procedures; as a result of this, the region was avoided in growing  $\text{In}_x\text{Se}_y$  thin films.

During the reverse cycle process, elemental  $\text{In}$  and  $\text{In}$  from  $\text{In}_x\text{Se}_y$  starts to dissolve into the electrolytic bath at low cathodic voltages around 1650 mV. At this cathodic voltage, the deposition current becomes equal to dissolution current. The negative broad peak at cathodic voltage around 300 mV can be attributed to the dissolution of  $\text{Se}$  from the glass/FTO cathode.

### 3.2 X-ray diffraction

The structural properties of the  $\text{In}_x\text{Se}_y$  layers were studied using X-ray diffraction (XRD) in the  $2\theta$  range ( $20$  to  $70^\circ$ ). This work was carried out by growing  $\text{In}_x\text{Se}_y$  layers for one hour on glass/FTO substrates at different growth voltages within the identified approximate deposition voltage obtained from the voltammogram scan. Ten  $\text{In}_x\text{Se}_y$  layers were grown at different growth voltages in step of 10 mV in order to find near stoichiometric growth voltage range for the deposition of  $\text{In}_x\text{Se}_y$  semiconductor thin films. After growth, the samples were cleaned with deionised water and dried in air.

Each of the ten as-deposited samples grown at different cathodic voltages were divided into 2 parts, The first set of ten samples was left in the as-deposited (AD) state and the other set annealed at  $300^\circ\text{C}$  for 10 minutes in air. The layers were then rinsed with deionised water and dried in air. Figure 3 shows the XRD spectra for (a) as-deposited and (b) annealed  $\text{In}_x\text{Se}_y$  layers grown at different growth voltages close to the transition or inversion voltage ( $V_i$ ).

The  $V_i$  voltage in this case was found to be  $\sim 1810$  mV as will be discussed later under the PEC cell measurements. The  $V_i$  is the voltage at which the conductivity type of the material changed from p-type to n-type or vice versa. The XRD spectrum for the glass/FTO substrate was included in both as-deposited and annealed samples for easy comparison. Results from both as-deposited (Figure 3(a)) and annealed (Figure 3(b)) show that the material is amorphous with no  $\text{In}_x\text{Se}_y$  related peaks. All observed peaks are due to the underlying glass/FTO substrate under the growth conditions used in this experiment. The growth of both polycrystalline [3,20] and amorphous [6,21]  $\text{In}_x\text{Se}_y$  have been reported in the literature.

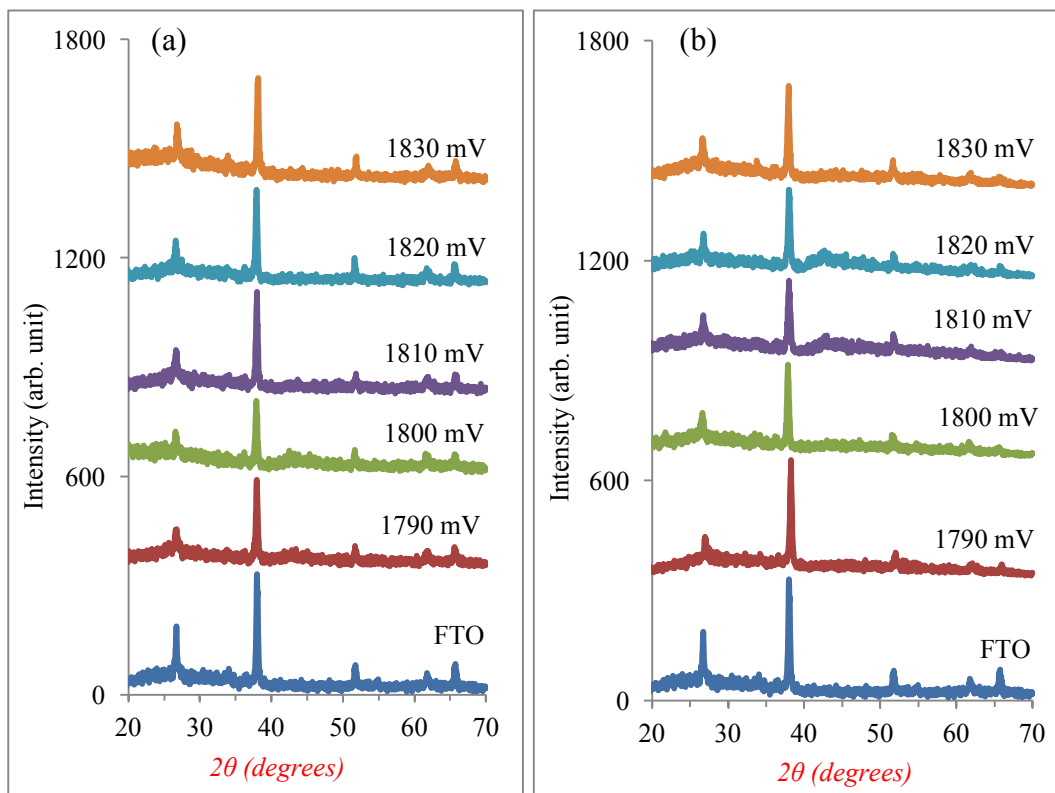


**Figure 3:** XRD patterns for (a) as-deposited and (b) annealed  $\text{In}_x\text{Se}_y$  layers grown at different voltages; annealing was carried out at  $300^\circ\text{C}$  for 10 minutes in air.

### 3.3 Optical absorption study

This investigation was carried out on the glass/FTO/ $\text{In}_x\text{Se}_y$  layer grown at the transition voltage (1810 mV) to study the bandgap of the  $\text{In}_x\text{Se}_y$  layers in both as-deposited and annealed conditions. After growth, the sample was rinsed with deionised water and dried in air. The bandgaps of both as-deposited and heat-treated layers were estimated using Tauc method [22] from the plot of absorption square versus photon energy ( $A^2$  vs.  $h\nu$ ) and by extrapolating the straight line portion of the absorption square ( $A^2$ ) to photon energy ( $h\nu$ ) axis (at  $A^2=0$ ).

Figure 4(a) and 4(b) illustrates the absorption square versus photon energy ( $A^2$  vs  $h\nu$ ) for as-deposited and annealed samples. The estimated bandgap in the as-deposited sample is 2.45 eV but after annealing it shifted to 2.90 eV. Similar bandgaps were reported for  $\text{In}_x\text{Se}_y$  thin films [23]. The increase in the bandgap after annealing could be due to material re-structuring and annihilation of defect structures or could be due to loss of material thereby reducing layer thickness.

The structural and optoelectronic properties of materials are dependent on parameters such as layer thickness, annealing temperature and annealing time. One of the advantages offered by electrodeposition as a semiconductor growth technique is the ease in the control of growth parameters. The large bandgap achieved in these layers could be very beneficial when incorporated as a buffer or window layers in both heterojunction and/or graded bandgap solar cell devices. This allows the incident photons to reach the device junction and improve photovoltaic activity within the device.

### 3.4 Morphological study

Scanning electron microscopy (SEM) technique was used to investigate the effect of annealing temperatures on the surface morphology of  $\text{In}_x\text{Se}_y$  layers. Figure 5 shows SEM images of glass/FTO/ $\text{In}_x\text{Se}_y$  layers for (a) as-deposited and (b) annealed at  $300^\circ\text{C}$  for 10 minutes in air.

The as-deposited sample is seen to have uniformly covered and densely packed spherical agglomerations of the films on the glass/FTO substrate. In this sample few pinholes are observed which could be due to cleaning process. After annealing (Figure 5(b)), it is observed that the agglomerations became relatively denser and uniform than in the as-deposited sample. However, few scattered pinholes were observed in both samples possibly due to the cleaning process.

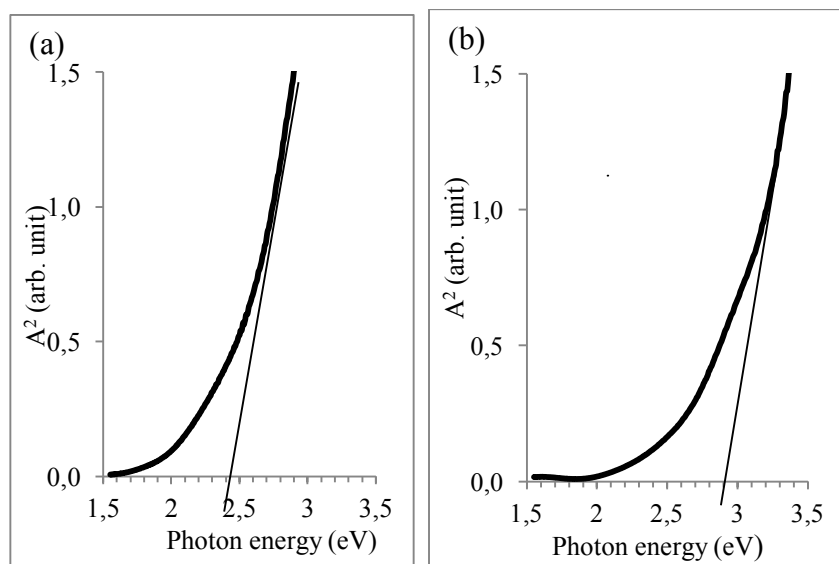


**Figure 4:** Optical absorption spectra (a) as-deposited and (b) annealed samples; annealing was carried out at 300°C for 10 minutes in air.

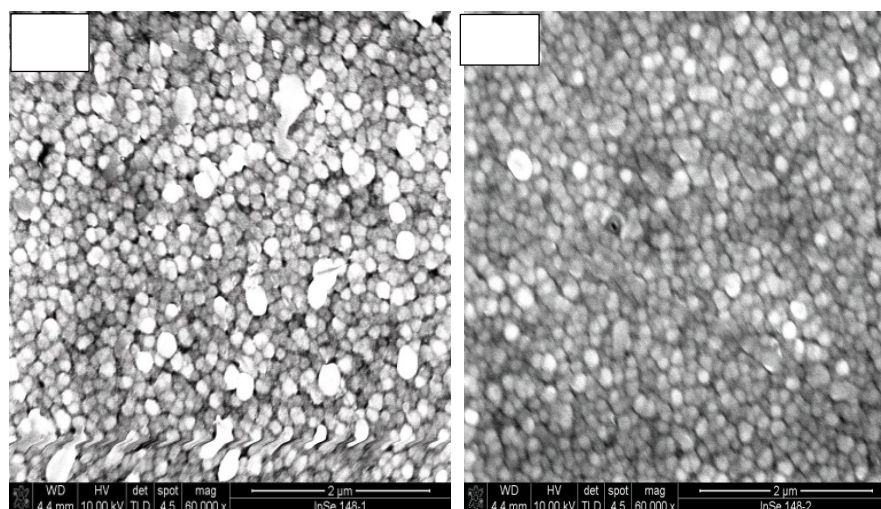


**Figure 5:** SEM images of  $\text{In}_x\text{Se}_y$  layers for (a) as-deposited and (b) annealed samples; annealing was carried out at 300°C for 10 minutes in air.

### 3.5 Photoelectrochemical cell measurements

Photoelectrochemical (PEC) cell measurements were performed on the layers to confirm their electrical conductivity type. The experiments were carried out by growing ten  $\text{In}_x\text{Se}_y$  layers on glass/FTO substrates at growth voltages in the range (1750-1850) mV earlier estimated from the voltammogram shown in Figure 2. Figure 6 shows the plot of PEC signal vs. growth voltage of  $\text{In}_x\text{Se}_y$  layers grown in steps of 10 mV in both as-deposited and annealed conditions. In the as-deposited layers, it is observed that at lower voltages (1750-1800) mV, the layers were Se-rich and p-type in electrical conduction while at higher growth voltages (1810-1850) mV; the layers were In-rich and n-type in electrical conduction. Between these two regions, there exists an inversion voltage ( $V_i$ ) where the electrical conduction type changes from p-type to n-type or from n-type to p-type. The obtained  $V_i$  in this work is ~1810 mV. Therefore materials grown at voltages lower than 1810 mV are p-type due to Se-richness while those grown above 1810 mV are n-type due to In-richness.

It is observed that by simply changing the growth voltage, the conductivity type of  $\text{In}_x\text{Se}_y$  can be altered by intrinsic doping or doping by varying the composition.

It is also important to point out that the value of the  $V_i$  can shift depending on parameters such as selenium concentration, growth temperature, pH and stirring rate. After annealing, all layers move to n-type as can be observed in Figure 6. This change could be as a result of defects redistribution and/or annealing out defects in the films during heat treatment. Though electrodeposition provides the room for the deposition of both n-type

and p-type in various semiconductors such as CdTe [24], ZnSe [25], ZnTe [26], ZnS [27], Based on the literature search, this is the first time the growth of both n-type and p-type  $\text{In}_x\text{Se}_y$  semiconductor is demonstrated from a single electrolyte. Work is on-going on the incorporation of these layers in CdTe-based graded bandgap solar cell devices.

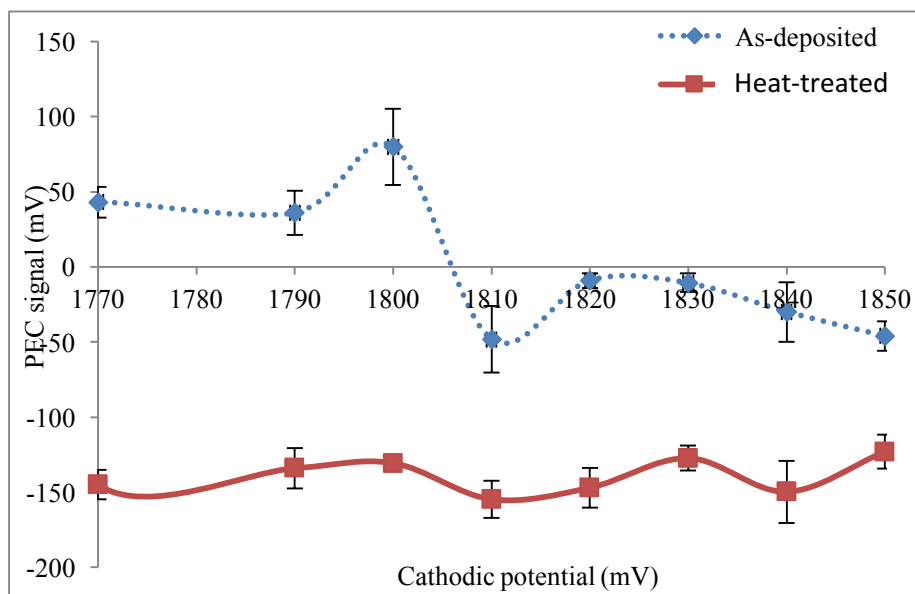


**Figure 6:** PEC signal vs. growth voltage for as-deposited and heat-treated  $\text{In}_x\text{Se}_y$  layers grown at different growth voltages.

## Conclusions

The electroplating and characterisation of  $\text{In}_x\text{Se}_y$  thin films were successfully carried out from aqueous acidic electrolyte using a simple 2-electrode electrochemical deposition technique. XRD studies showed that the material grown is amorphous in both as-deposited and after heat treatment. PEC cell measurements showed that both n-type and p-type  $\text{In}_x\text{Se}_y$  thin films were obtained by varying the growth voltage. Surface morphology for both as-deposited and heat-treated  $\text{In}_x\text{Se}_y$  thin films showed slight improvement which further indicates the amorphous nature of these layers. The energy bandgap of the representative sample grown at 1810 mV in both as-deposited and annealed condition showed 2.45 and 2.90 eV respectively.

**Acknowledgement**—The authors appreciate the contributions by Drs F. Fauzi, H.I. Salim and N.A. Abdul-Manaf. Our special appreciation goes to Prof. I.M. Dharmadasa for guidance in the course of our research programmes. The main author wish to thank Petroleum Technology Development Fund (PTDF), Abuja, Nigeria for sponsorship and Gombe State University is acknowledge for financial assistance.

## Reference

1. M.L. Madugu, L. Bowen, O.K. Echendu, I.M. Dharmadasa, *J. Mater. Sci. Mater. Electron.* 25 (2014) 3977–3983.
2. K. Yilmaz, *J. Ovonic Res.* 10 (2014) 67–73.
3. M. Parlak, Ç. Erçelebi, *Thin Solid Films.* 322 (1998) 334–339.
4. A. Segura, A. Chevy, J.P. Guesdon, J.M. Besson, *Sol. Energy Mater.* 2 (1980) 159–165.
5. A. Ates, M. Kundakci, Y. Akaltun, B. Gurbulak, M. Yildirim, *Phys. E Low-Dimens Syst. Nanostruct.* 36 (2007) 217–220.
6. A.F. Qasrawi, *J. Mater. Sci. Mater. Electron.* 12 (2001) 473–476.
7. G. Gordillo, C. Calderon, C. Quinonez, *Proceeding of 3rd World Energy Conference on Photovoltaic Energy Conversion*, May 11–18, 2003, Osaka, Japan., in: n.d.
8. M.A. Kenawy, M.A. Afifi, H.A. Zayed, *Thin Solid Films*, 200 (1991) 203–210.
9. A.F. Qasrawi, *Phys. Scr.* 89 (2014) 065802.
10. A.F. Qasrawi, *J. Electron. Mater.* 42 (2013) 1033–1036.
11. S. Massacesi, S. Sanchez, J. Vedel, *J. Electroanal. Chem.* 412 (1996) 95–101.
12. S. Marsillac, A.M. Combot-Marie, J.C. Bernède, A. Conan, *Thin Solid Films.* 288 (1996) 14–20.

13. A. Ateş, M. Kundakçı, A. Astam, M. Yıldırım, *Phys. E Low-Dimens Syst. Nanostruct.* 40 (2008) 2709–2713.
14. K. Saiki, K. Ueno, T. Shimada, A. Koma, *J. Cryst. Growth.* 95 (1989) 603–606.
15. J.F. Sánchez-Royo, A. Segura, O. Lang, E. Schaar, C. Pettenkofer, W. Jaegermann, R. Roa, A. Chevy, *J. Appl. Phys.* 90 (2001) 2818–2823.
16. O.A. Balitskii, V.P. Savchyn, V.O. Yukhymchuk, *Semicond. Sci. Technol.* 17 (2002) L1–L4.
17. M.A. Green, K. Emery, Y. Hishikawa, W. Warta, E.D. Dunlop, *Prog. Photovolt. Res. Appl.* 24 (2016) 905–913.
18. M. Konagai, Y. Ohtake, T. Okamoto, *Mater. Res. Soc. Symp. Proc.* 426 (1996) 153.
19. P. Vanysek, *Handbook of chemistry and physics*, CRC Press LLC, 2000.
20. C. Viswanathan, G.G. Rusu, S. Gopal, D. Mangalaraj, Sa. Narayandass, *J. Optoelectron Adv. M* 7 (2005) 705–711.
21. A. Chaiken, K. Nauka, G.A. Gibson, H. Lee, C.C. Yang, J. Wu, J.W. Ager, K.M. Yu, W. Walukiewicz, *J. Appl. Phys.* 94 (2003) 2390.
22. J. Tauc, *Phys. Stat. Sol.* 15 (1966) 627
23. A. Mohan, J. Suthagar, T. Mahalingam, *Nanomater. Appl. Proc* 2 (2013) 3–7.
24. H.I. Salim, V. Patel, A. Abbas, J.M. Walls, I.M. Dharmadasa, *J. Mater. Sci. Mater. Electron.* 26 (2015) 3119–3128.
25. P.A. Samantilleke, M.H. Boyle, J. Young, I.M. Dharmadasa, *J. Mater. Sci. Mater. Electron.* 9 (1998) 231–235.
26. O.I. Olusola, M.L. Madugu, N.A. Abdul-Manaf, I.M. Dharmadasa, *Curr. Appl. Phys.* 16 (2016) 120–130.
27. M.L. Madugu, O.I.O. Olusola, O.K. Echendu, B. Kadem, I.M. Dharmadasa, *J. Electron. Mater.* 45 (2016) 2710–2717.

(2018) ; <http://www.jmaterenvirosci.com>